

AN EXPERIMENTAL STUDY OF A NEW ENTROPY-BASED SAR AUTOFOCUS TECHNIQUE

Robert L. Morrison, Jr. and David C. Munson, Jr.

The University of Illinois at Urbana-Champaign
Department Of Electrical and Computer Engineering
Coordinated Science Laboratory

ABSTRACT

The Stage By Stage Approaching (SSA) entropy minimization approach to synthetic aperture radar (SAR) autofocus is a modern and innovative technique, which has not been compared with other approaches, to date. We provide such a comparison and show that SSA is a most promising autofocus method. In this paper, we evaluate the merit of this algorithm through comparison with the established Phase Gradient Autofocus (PGA) algorithm on both simulated and real SAR data.

1. INTRODUCTION

In a Synthetic Aperture Radar (SAR) imaging scenario, proper demodulation of radar returns requires knowledge of the distance between the radar platform and the scene being imaged. When this distance is not known accurately, a phase error results that corrupts the imaging data. The phase error function $\phi_e(X)$, varying with each received echo (in the cross-range frequency dimension X), acts as a blurring filter, defocusing the radar image. The corrupted Fourier imaging samples $\tilde{G}(X, Y)$ are related to the uncorrupted samples $G(X, Y)$ by

$$\tilde{G}(X, Y) = G(X, Y)e^{-j\phi_e(X)}, \quad (1)$$

where Y represents the range spatial frequency dimension. Autofocus algorithms create an estimate of the phase error function, $\hat{\phi}_e(X)$, to correct the defocused image.

Several autofocus algorithms have been presented in the literature over the past 20 years. Highly regarded among these is the widely utilized Phase Gradient Autofocus (PGA), published by Eichel, Ghiglia, and Jakowatz in 1989 [1,2]. PGA estimates phase differences between columns of Fourier data, and then integrates to produce an estimate of the phase error function [2]. A more recent algorithm is Stage By Stage Approaching (SSA), published by Li, Guosui, and Ni in 1999 [3]. SSA determines the phase error estimate that minimizes the entropy of an image. The algorithm is innovative because it uses a search technique that does not require the computation of a gradient [3]. However, the authors of the algorithm have made no comparison with other

established methods. Thus, its performance is unknown. In this paper, we compare the performance of SSA with that of PGA. This comparison is made quantitatively, using both simulated data, and real SAR data provided by Sandia National Laboratories. Our results show that SSA works well in comparison to the state-of-the-art PGA. However, SSA is more computationally demanding.

2. PGA VS. SSA

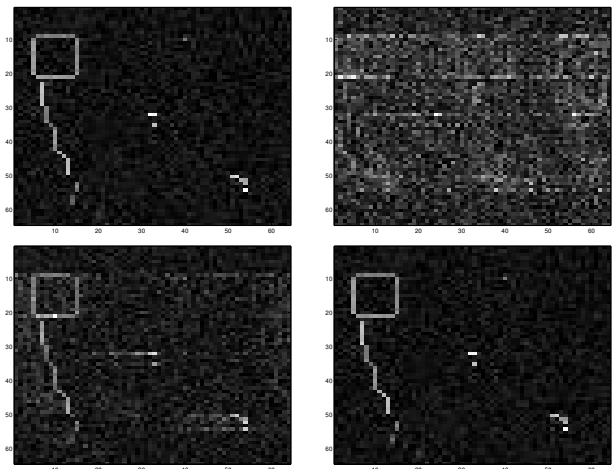


Fig. 1. Synthesized test image (clutter variance 0.15). (a) Top left: original image. (b) Top right: corrupted image. (c) Bottom left: PGA reconstruction. (d) Bottom right: SSA reconstruction.

Fig. 1(a) shows the magnitude of a synthesized test image. We will refer to this as the original, or uncorrupted image, obtainable in the absence of phase error. The image was formed by defining several targets against a backdrop of uniformly distributed clutter. A random phase, uniformly distributed between $-\pi$ and π and independent from pixel to pixel, was applied in the spatial domain to model the complex reflectivity of background terrain. The corrupt image of Fig. 1(b) was formed by applying a white phase

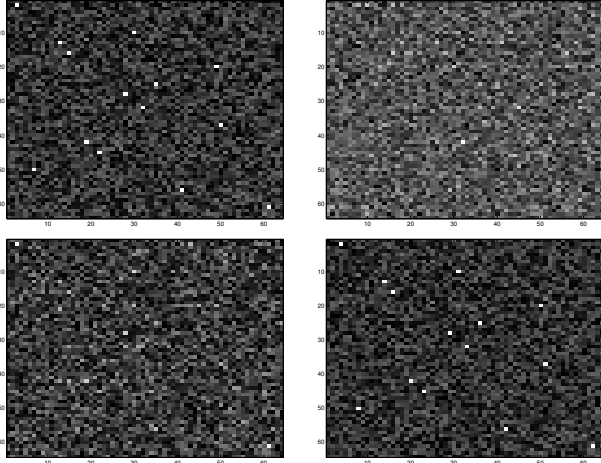


Fig. 2. Synthesized point target image (clutter variance of 0.01333). (a) Top left: original image. (b) Top right: corrupted image. (c) Bottom left: PGA reconstruction. (d) Bottom right: SSA reconstruction.

error function, uniformly distributed in $-\pi$ and π and varying only in the cross-range dimension, to the Fourier data of the original image. The effect of this phase error function in the spatial domain is that of a blurring filter with a Rayleigh distributed impulse response. A plot of the magnitude of this blurring kernel reveals several dominant point-like impulses, such that the resulting corrupted image is a superposition of scaled and shifted replicas of the real and imaginary components of the original image. The application of the PGA and SSA algorithm to the corrupted image of Fig. 1(b) produces the images of Fig. 1(c) and Fig. 1(d), respectively. The SSA reconstruction is nearly identical to the original image. The PGA reconstruction, in contrast, reveals misleading echoes and obscured features.

Fig. 2(a) shows the magnitude of a second test image. This image is composed of fourteen real-valued point targets surrounded by uniformly distributed clutter. A corrupted version of this image, formed by perturbing the Fourier data of the original image with a white phase error function (again uniformly distributed between $-\pi$ and π and varying only in cross-range), is displayed in Fig. 2(b). Applying PGA and SSA to the corrupted image produces the reconstructions shown in Figs. 2(c) and 2(d), respectively. Inspection of these images reveals that SSA produces a more accurate reconstruction than PGA. The point targets in the PGA image have been blurred in the cross-range, and several false targets appear.

To quantitatively compare the performance of PGA and SSA, we plotted a measure of quality for both algorithms as a function of the clutter variance. This plot is displayed in Fig. 3. A set of images was formed with the fourteen

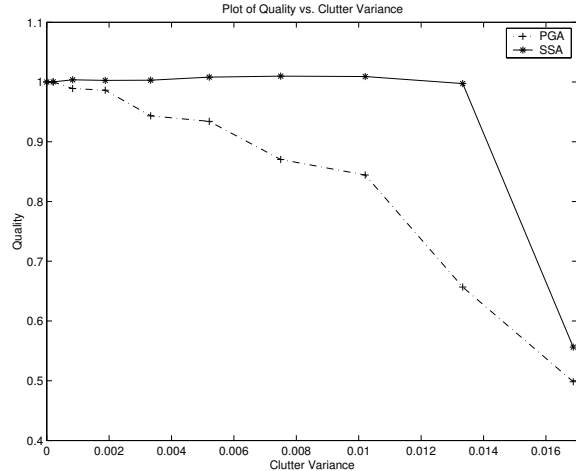


Fig. 3. A plot of the quality measure, the average of the magnitudes of the 14 point targets in the reconstructed images of Figure 2, versus the input clutter variance, for both PGA and SSA.

point targets of Fig. 2, with each image assigned a different clutter variance. The quality measure was defined to be the average of the magnitudes of the fourteen point targets in the PGA and SSA reconstructed images. Fig. 3 shows that SSA performs consistently well over a wide range of clutter variances, but then breaks down above a certain threshold. The performance of PGA, in contrast, progressively degrades with increasing clutter variance.

The results outlined in the previous paragraphs illustrate the potential of SSA on simulated data. We will now demonstrate the utility of SSA on real data. Sandia National Laboratories, which developed the PGA algorithm, has provided us with real SAR images of a grassy scene. The first is the uncorrupted image, shown in Fig. 4. The second is a corrupted version of that image (Fig. 5), exhibiting the effect of an unknown phase function. The third image is a PGA reconstruction of the corrupted image (Fig. 6), using Sandia National Laboratories version of PGA. Fig. 7 shows a reconstruction of the grassy scene produced using our version of SSA. The uncorrupted grassy scene of Fig. 4 contains many point-like scatterers. The full-sized (512 by 512 pixels) image displayed with an appropriate color map on a computer monitor reveals the point-like features much more distinctly than the black and white image presented here. However, several prominent scatterers, such as the points at coordinates (234,200) and (259,198), are evident by inspection of the figure.

We have magnified an interesting portion of the grassy image to provide a basis for qualitative comparison. This excerpt, displayed in Fig. 8, reveals row-like features. These ‘rows’ are defined more distinctly in the SSA reconstruc-

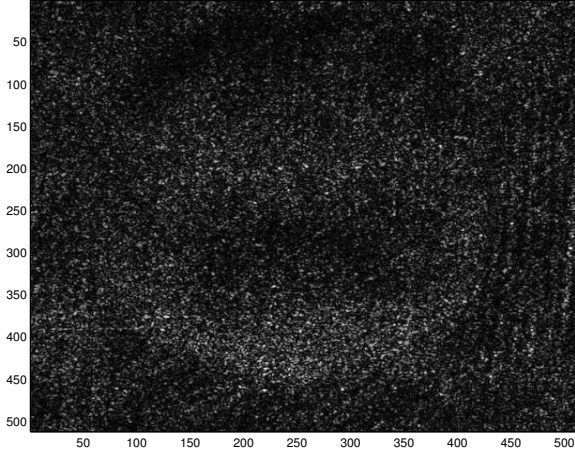


Fig. 4. The uncorrupted SAR image of a grassy scene.

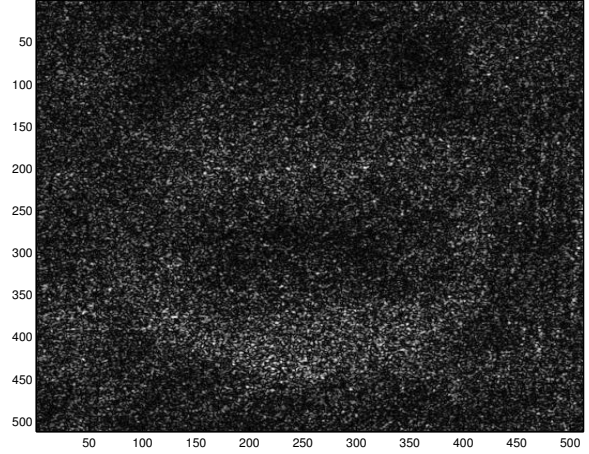


Fig. 6. PGA reconstruction of the grassy scene.

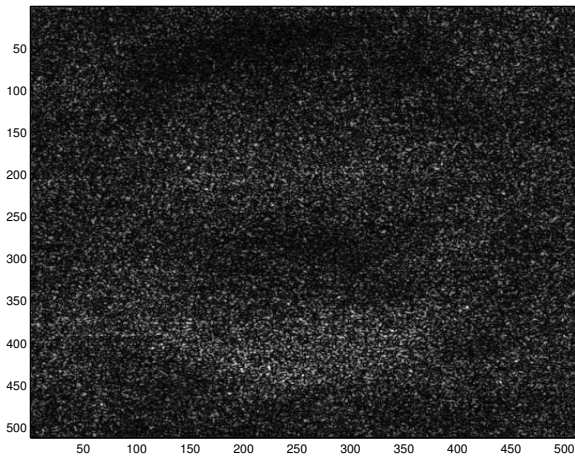


Fig. 5. The corrupted image of the grassy scene.

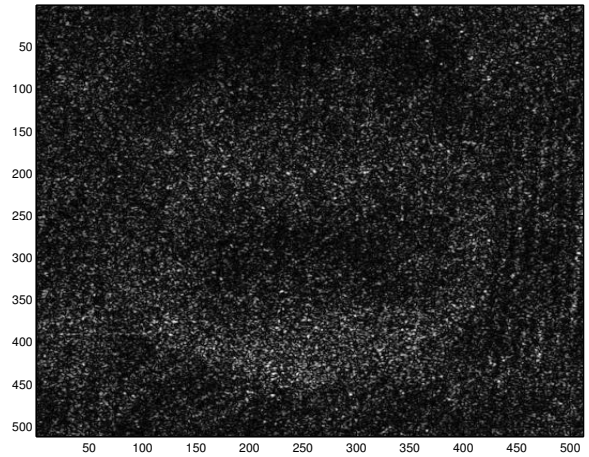


Fig. 7. SSA reconstruction of the grassy scene.

tion. In the PGA reconstruction the rows blur together. The target-like features depicted in the uncorrupted image segment are obscured in the PGA image, and extraneous features abound. The SSA reconstruction, in contrast, yields a faithful restoration of prominent features.

To quantitatively compare the performance of PGA and SSA on the grassy image, we analyzed correct and incorrect reconstructions of point-like features. The point-like scatterers found in these images were considered ‘targets’. We applied a threshold to the original, SSA corrected, and PGA corrected images. If the pixel value in the images was greater than the threshold, we noted the coordinates of that pixel, and considered that pixel to be a target (if multiple adjacent pixels exceeded the threshold, only one of the pixels was considered a unique target). Five lists were constructed: targets in the original image, targets de-

tected correctly with PGA, targets detected incorrectly with PGA (false alarms), SSA correct detections, and SSA false alarms. Correct detection means a target detected by either PGA or SSA matched a target in the original image (up to a small euclidean distance), while a false alarm implies no match. The detection statistics are summarized in the following table.

Target Detection Statistics (Target Threshold = 200)

	SSA	PGA
Distinct Targets (63 in original image)	79	46
Correct Detections	57	25
False Alarms	22	21

The probability of correct detection is expressed as the conditional probability that a system detects a target given that a target is actually present. Likewise, the probability

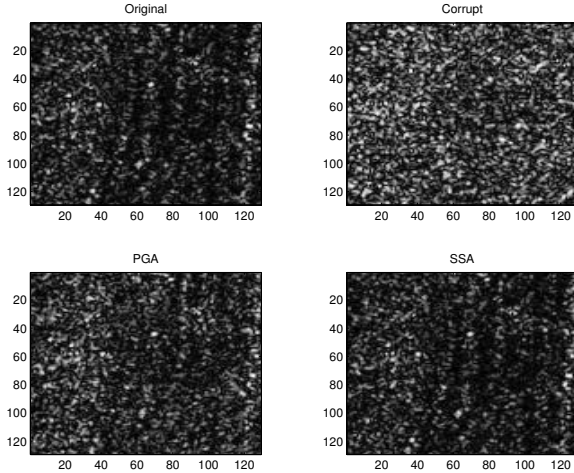


Fig. 8. Enlarged portion of grassy SAR image. (a) Top left: original image. (b) Top right: corrupted image. (c) Bottom left: PGA reconstruction. (d) Bottom right: SSA reconstruction.

of false alarm is defined as the conditional probability that the reconstructed image indicates a target when no corresponding target exists in the original image. We considered the true targets to be those in the original image exceeding a threshold of 200. We then determined the probability of detection versus false alarm for PGA and SSA by applying 50 thresholds in the range of 185 to 235 to the reconstructed imagery. The resulting plot is displayed in Fig. 9. This plot indicates that the SSA algorithm achieves a superior probability of detection versus false alarm.

3. EFFICIENT IMPLEMENTATION OF SSA

We believe that SSA has great potential as a powerful and robust autofocus tool. However, the computational expense of the algorithm is a major drawback that must be addressed before SSA can be placed into widespread use. Our fastest implementation of SSA still requires approximately ten times the computational time of PGA for images of size 512 by 512 pixels. We employed several expediting measures not explicitly mentioned in the original SSA paper [3]. The normalization step proposed by the authors in the entropy calculation is unnecessary in the actual implementation of SSA, which yields significant savings. This conclusion can be reached through Parseval's relation. More significantly, we determined that a complete one dimensional FFT is not required after every step in the algorithm.

We have explored variation of the SSA algorithm, including limiting the number of iterations, and a multiresolution scheme, to reduce computational expense. We have also experimented with alternative cost functions in place of entropy, proposed by the authors in [3]. These cost functions are less computationally expensive to evaluate, and

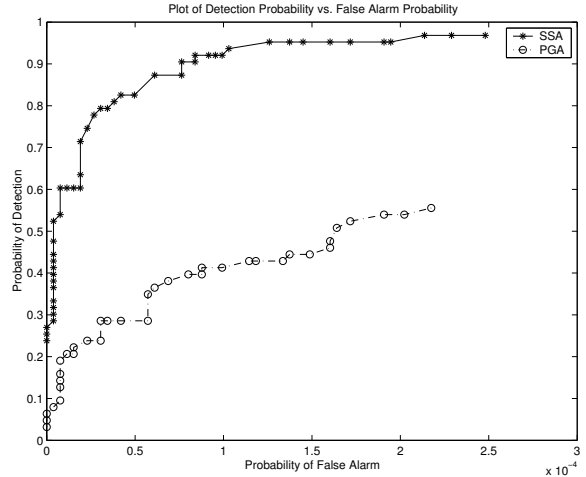


Fig. 9. Plots of probability of detection vs probability of false alarm for targets in the grassy SAR image, for both PGA and SSA.

lend themselves to possible time-saving approximations (such as calculating only a cost function increment between steps) more easily. One measure, the ratio of the standard deviation to the mean of the image intensity, produced results nearly identical to entropy on the simulated image of Fig. 1, but produced a completely erroneous reconstruction of the grassy image. So far, the entropy cost function has produced the best overall results.

ACKNOWLEDGEMENTS

The authors are indebted to Dr. Charles Jakowatz, Jr. of Sandia National Laboratories for supplying the real SAR images presented in this paper. The authors also thank Jeffrey Brokish, of the University of Illinois, for his advice and assistance in this work. Portions of this research were supported by AFOSR/DARPA contract DAAD19-00-C-0099.

REFERENCES

- [1] P. H. Eichel, D. C. Ghiglia, and C. V. Jakowatz, Jr., "Speckle Processing Method for Synthetic Aperture Radar Phase Correction," *Optics Letters*, Vol. 14, pp. 1101-1103, January 1989.
- [2] C. V. Jakowatz, Jr., D. E. Wahl, P. H. Eichel, D. C. Ghiglia, P. A. Thompson, *Spotlight-Mode Synthetic Aperture Radar: A Signal Processing Approach*. Boston: Kluwer Academic Publishers, 1996.
- [3] L. Xi, L. Guosui, J. Ni, "Autofocusing of ISAR Images Based on Entropy Minimization," *IEEE Transactions on Aerospace and Electronic Systems*, Vol. 35, pp. 1240-1252, October 1999.